Title

Measurements of the Cosmic Microwave Background Temperature at 1.47 GHz

Journal

Astrophysical Journal, 409

Authors

Bensadoun, M.
Bersanelli, M.
Amici, Giovanni De
et al.

Publication Date

1992-07-01

Measurements of the Cosmic Microwave Background Temperature at 1.47 GHz

M. Bensadoun(1), M. Bersanelli(1)(2), G. De Amici(1), A. Kogut(3), M. Limon(1),

S. M. Levin(1)(4), G. F. Smoot(1), and C. Witebsky(1)

ABSTRACT

We have used a radiofrequency-gain total-power radiometer to measure the intensity of the cosmic microwave background (CMB) at a frequency of 1.47 GHz (20.4 cm wavelength) from White Mountain, California in September 1988 and from the South Pole, Antarctica in December 1989. The CMB thermodynamic temperature, T_{CMB}, is 2.27 ± 0.25 K (68% C.L.) measured from White Mountain and 2.26 ± 0.21 K from the South Pole site. The combined result is 2.27 ± 0.19 K. The correction for galactic emission has been derived from scaled low-frequency maps and constitutes the main source of error. The atmospheric signal is extrapolated from our zenith scan measurements at higher frequencies. These results are consistent with our previous measurement at 1.41 GHz (Levin *et al.* 1988) and ~2.5 σ from the 2.74 ± 0.01 K global average CMB temperature.

subject headings: cosmic background radiation; cosmology; galactic emission

(1) Space Sciences Laboratory and Lawrence Berkeley Laboratory, M/S 50-351,
University of California, Berkeley CA 94720, USA

(2) Istituto di Fisica Cosmica, CNR, via Bassini 15, 20133 Milano, Italia

(3) Universities Space Research Association, Code 685.9, NASA Goddard Space Flight Center,
Greenbelt, MD 20771, USA

(4) present address: JPL, M/S 169-506, Pasadena, CA 91109, USA

1. INTRODUCTION

The spectrum of the cosmic microwave background (CMB) reflects physical conditions and processes in the early universe (*e.g.* Burigana *et al.* 1991 and references therein). Recent results from the FIRAS experiment aboard the COBE satellite (Mather *et al.* 1990) have established the blackbody nature of the spectrum above 30 GHz and focused attention on the low-frequency spectrum. Generally, energy transferred to the CMB photons at early times, at redshift z in the range $10^7 \geq z \geq 10^4$, causes a low-frequency ($\nu \leq 10$ GHz) distortion in the spectrum. One such distortion is a chemical potential distortion which deviates most from black body in the 1-2 GHz range for $\Omega_b \sim 0.1$, where Ω_b is the ratio of the baryon density of the universe to the critical density (Burigana *et al.* 1991). Other types of distortions, such as those due to particle decay (reverse chemical potential evolution) (Silk and Stebbins 1983) or free-free scattering (Bartlett and Stebbins, 1990), can also be large in this frequency range. Precise measurements in the 1-2 GHz range combined with the precise high-frequency measurements now available are an ideal probe of these distortions. A measurement near 1.5 GHz is low enough in frequency to allow significant distortions but high enough that the foreground galactic signal is still a factor of three weaker than the CMB.

Since 1982 we and our collaborators have been making measurements of the CMB spectrum at frequencies between 0.6 and 90 GHz (Smoot *et al.* 1983 & 1985, Kogut *et al.* 1991). In 1986 we made a measurement at 1.41 GHz (Levin *et al.* 1988); based on that experience, we built a new radiometer and cold load calibrator to make measurements at 1.47 GHz.

In September 1988, our group made CMB measurements at 3.8 GHz (De Amici *et al.* 1990), 7.5 GHz (Kogut *et al.* 1990), and 1.47 GHz from White Mountain (WM). In December 1989, we repeated the 3.8 GHz (De Amici *et al.* 1991), 7.5 GHz (Levin *et al.* 1992), and 1.47 GHz measurements from the South Pole (SP) and a collaborating group from the University of Milano made measurements at 0.82 and 2.5 GHz (Sironi *et al.* 1992). This is a report on the 1988 and 1989 measurements at 1.47 GHz.

2. CONCEPT OF THE MEASUREMENT

The measurement is performed with a total-power radiometer whose output signal, S, is proportional to the power, P, entering the antenna aperture; the output is calibrated in units of antenna temperature, T_A.[5]

The experiment consists of comparing the signal from the zenith with that from a large, liquid-helium cooled, cold-load calibrator (CL) whose antenna temperature, $T_{A,\mathrm{load}}$, is precisely known. The antenna temperature of the zenith, $T_{A,\mathrm{zenith}}$, is

$$T_{A,\mathrm{zenith}} = G\,(S_{\mathrm{zenith}} - S_{\mathrm{load}}) + T_{A,\mathrm{load}} - \Delta T_{\mathrm{inst}} - \Delta T_{A,\mathrm{joint}}, \tag{1}$$

where G is the gain calibration coefficient for the radiometer, $S_{\mathrm{zenith}}-S_{\mathrm{load}}$ is the measured signal difference between the zenith and the cold load, ΔT_{inst} is the correction for any changes in the radiometer signal associated with its inversion during the measurement and $\Delta T_{A,\mathrm{joint}}$ is the differential temperature contribution from the imperfect joint between the antenna and the cold load. The ΔT_{inst} can be due to orientation-dependent changes in gain, system temperature, physical temperature, reflection and insertion loss of the front-end of the radiometer, and electrical effects.

The temperature of the CMB is found by accounting for all non-cosmological contributions to $T_{A,\mathrm{zenith}}$. These include emission from the galaxy, atmosphere, ground, the sun, and man-made radio-frequency interference (RFI):

$$T_{A,\mathrm{zenith}} = T_{A,\mathrm{sky}} + T_{A,\mathrm{atm}} + T_{A,\mathrm{ground}} + T_{A,\mathrm{sun}} + T_{A,\mathrm{RFI}}\,, \tag{2}$$

---

[5] T_A is defined by the relation $T_A \equiv P/kB = T_\nu\,(exp(T_\nu/T) - 1)^{-1}$, where B is the bandwidth, $T_\nu = h\nu/k = 0.706$ K at 1.47 GHz, and h and k are the Planck and Boltzman constants, respectively.

where the sky temperature, $T_{\mathrm{A,sky}}$, is defined as:

$$T_{\mathrm{A,sky}} = T_{\mathrm{A,CMB}} + T_{\mathrm{A,gal}}$$

The atmospheric signal is found by extrapolation from measurements at higher frequencies. Atmospheric attenuation is neglected in this discussion, but not in the analysis. The ground signal is found by convolving the measured antenna gain pattern with the ground emission. The terms in equations (1) and (2) are discussed in detail in § 5. Galactic emission is calculated from low-frequency maps and the observed spectral index; a detailed discussion of the galactic signal is given in § 7. The signals from the atmosphere, ground, and cold load are constant during each measurement; the galactic signal varies as the earth rotates.

3. INSTRUMENT DESCRIPTION

The radiometer uses an E-plane corrugated horn antenna (Witebsky *et al.* 1987) (46 x 52 cm aperture) and an rf-gain total-power receiver (see Figure 1 and Table 1). The signal enters the antenna and passes through a waveguide-coaxial transition into coaxial cable. A 1.0-1.6 GHz bandpass filter cuts out low-frequency RFI signals to avoid saturation of the second RF amplifier. A 6-stage Yttrium Iron Garnet (YIG) filter defines a 26 MHz instantaneous bandpass. During CMB measurements, the YIG filter center frequency is swept at 1 GHz/s from 1.375 to 1.575 GHz to synthesize a bandwidth of 200 MHz, centered at 1.475 GHz. The gain-weighted band center is 1.471 GHz. For each amplifier, the output signal level is more than 20 dB below the 1 dB compression point.

The radiofrequency signal is detected by a power-law detector diode. The detector diode output is in the range 1.2 – 6.5 mV when the radiometer observes 4 – 300 K targets. Saturation of the detector diode results in a 2.0 ± 0.9 % gain correction derived from measurements of the diode linearity. The DC signal is then amplified by either 1000 (low-gain scale) or 2500 (high-gain scale). The signal is integrated for 2 seconds, offset by –10 V and recorded. The –10 V offset is stable to better than 1 part in 10^4 over a period of a few minutes.

We measure the radiometer gain and system temperature by comparing the signals from the ambient temperature blackbody target and from the cold load. The ambient temperature target is a 60 cm x 60 cm blackbody absorber enclosed in a thermally insulated, rf-tight box which covers the antenna aperture during gain calibration.

4. OBSERVATIONS

The RFI emissions associated with populated areas require us to choose a remote site. A low horizon is necessary to reduce the ground signal to an acceptable level. The magnitude of atmospheric emission and the characteristic roll-off frequency of the emission both decrease with altitude necessitating a high-altitude site. In addition, we need a region of sky with minimal galactic emission to be overhead during the observations.

During CMB measurements, we surrounded the antenna aperture with a smooth-walled pyramidal ground screen to avoid the unacceptably large signal due to the ground emission seen by the antenna alone (~0.6 K). The E-plane sides of the sheet metal screen were equipped with quarter-wavelength traps to further reduce ground pick-up. Emission from the screen is included in $T_{\mathrm{A,ground}}$.

We calibrated the measurements with a cold load reference target optimized for operation in the 1 to 10 GHz range (Bensadoun *et al.* 1992). The absorber in the load consists of Emerson & Cuming Eccosorb VHP-12 (a carbon-loaded urethane foam, 30 cm thick) backed by 6 cm of Eccosorb LS. A 78-cm diameter, aluminum-foil-coated, fiberglass cylinder joined the absorber to the mouth of the cold load. Two 25-μm thick polyethylene windows prevented condensation inside the cold load and two Teflon-impregnated glass-cloth (Fluorglas) windows reduced the infrared heat leak to the LHe. Although similar to the cold load used in our earlier measurements (Smoot *et al.* 1983), the new cold load incorporates several changes important to calibration at 1.5 GHz. Most importantly, the absorber reflection is smaller and the radiometric wall has fewer discontinuities.

We also added a 1.5 m long extension to the antenna to make differential zenith scans; for these measurements, no absolute calibration was needed, but very low sidelobes were essential. With the extension attached to the mouth, the half-power beamwidth (HPBW) was ~15° and the gain was <–60 dB at angles >90° (Witebsky et al. 1987).

4.1 WHITE MOUNTAIN 1988

We observed from the Nello Pace Laboratory of the University of California White Mountain Research Station (latitude 37.6° N, 3800 m altitude). The site lies on the eastern slope of a ridge which rises 18° towards the northwest; the horizon is lower in all other directions.

We made CMB observations during 3 separate runs on 19 Sep 1988 (UT). The first run occured when the galactic plane was nearly overhead (~21^h right ascension) so we could gather data on galactic emission. The second and third runs observed regions of lower galactic emission (RA ~22^h to 2^h). During the same period, we made CMB, atmospheric and galactic measurements at 3.8 and 7.5 GHz.

During each 160 s CMB measurement cycle, we used the radiometer to measure the zenith-cold load difference on high gain, then measured the high gain to low gain ratio observing the cold load and finally calibrated in low gain. Each cycle measured the low gain once and the zenith-cold load temperature difference once. The ratio of gains was obtained from the ratio of the low-gain cold-load signal to the high-gain cold-load signal.

4.2 SOUTH POLE 1989

These measurements were made from a site 1.8 km from the Amundsen-Scott Research Station (latitude 90° S) at the geographic South Pole. Resting on 2.5 km of ice at an altitude of 2800 meters, the site had an ambient temperature ranging from –20° to -30° C at the time of the observations. Except for two small buildings and the apparatus at the site, the horizon was flat. The ice was a gray-body at an effective temperature of 225 ± 10 K. The South Pole site offered a better horizon, lower ground temperature and lower galactic signal than the White Mountain site but the lower altitude resulted in a larger atmospheric signal. We used the same pyramidal ground screen as at White Mountain, and added a 5 m high sheet metal screen to reduce solar radiation.

We made CMB observations at the South Pole during five separate runs on 16, 17, 18 and 19 Dec 1989 (UT) during periods when the screen shielded the radiometer from solar radiation. In order to reduce the galactic signal, we tipped the radiometer away from the galactic plane to a region of lower emission during four of the five runs.

We used the same CMB observing cycle at the South Pole as was used at White Mountain except that each cycle measured the zenith-cold load difference temperature on both high and low gain. The ratio of gains was measured independently many times during the observations.

5. CONTRIBUTIONS TO THE SKY TEMPERATURE $T_{A,sky}$

5.1 ATMOSPHERIC EMISSION $T_{A,atm}$

We attempted to measure atmospheric emission at 1.47 GHz by tipping the radiometer to correlate the signal with the increased air mass. Uncertainties in the ΔT_{inst} and the signal from the extension joint rendered these data useless. We obtained the atmospheric signal by extrapolating from our measurements at White Mountain and the South Pole at 3.8 GHz (De Amici *et al.* 1990, De Amici *et al.* 1991) and 7.5 GHz (Kogut *et al.* 1990, Levin *et al.* 1992).

The atmospheric signal at 1.47 GHz at our sites is due to resonant and non-resonant emission by the complex of pressure-broadened oxygen lines clustered near $\nu_0 = 60$ GHz. The amplitude of the O_2 emission depends on atmospheric pressure and temperature and varies slowly with time. Emission from the water line at 22 GHz contributes negligibly at both sites (Danese and Partridge, 1989) and, for scaling purposes, the atmosphere is dry. Over the range $1 < \nu < 10$ GHz, in the simple, dry-atmosphere model of Gordon (1967), the attenuation, α (dB/km), scales approximately as:

$$\alpha = A\gamma \frac{x(1+3x)}{g(1-3x)^2 + x(1-x)^2}, \qquad (3)$$

where $x = (\nu/\nu_0)^2$, $g = (\gamma/\nu_0)^2$, and A and γ are the pressure- and temperature-dependent amplitude and line-width parameters for oxygen. For the atmospheric pressure and temperature at our sites, $\gamma \leq 0.5$ GHz so that the roll-off in atmospheric emission occurs below 1.5 GHz.

We extrapolate the measured values according to equation (3), propagate the error in each measured datum and include the uncertainty in the model parameter γ. The extrapolations from 3.8 and 7.5 GHz are in agreement at each site. We take $T_{A,Atm}$ to be the mean value weighted by the uncorrelated measurement errors, with uncertainty given by the quadrature sum of the weighted measurement errors and the uncertainty in γ. The effect of the finite beam has been taken into account. At zenith angle z, the effect is given by $\langle f(z)\rangle$, the atmospheric path length (relative to the zenith) averaged over the beam. Table 2 shows the 3.8 and 7.5 GHz measured atmospheric emission, and $\langle f(z)\rangle$ and $T_{A,Atm}$ at 1.47 GHz.

This simple extrapolation from values measured at nearby frequencies agrees well with the empirical atmospheric attenuation model of Danese and Partridge (1989). Figure 2 summarizes the measured data, the two models and the calculated values at 1.47 GHz.

5.2 GROUND EMISSION $T_{A,\text{ground}}$

The ground radiates into the antenna side- and back-lobes, contributing to the zenith signal. We calculate the ground contribution by convolving the measured antenna beam pattern (Figure 3) with the ground. We take into account the surface reflection and temperature of the ground, and the horizon profile. The results are summarized in Table 3. The co-polarized response in between the E- and H-planes is generally lower than in either the E- or H-planes, resulting in a correction by a factor of 0.87 ± 0.13 to the ground signal at both sites. Other uncertainties (and the uncertainty in the quantity) arise from the horizon elevation profile (±2°), the HPBW of the gain pattern (±2°), the relative gain of side- and back-lobes (±1dB), and the cross-polarized response (< -20dB).

We set a lower limit on the ground contribution from measurements of the residual ground radiation. The tests consist of shielding the aperture edge from ground radiation incident from below (diffraction test), extending the reflecting surface of the shield or extension (extension test) or covering part of the ground with a reflector.

The gain-weighted solid angle subtended by the ground screen is ~1.4% and the average emissivity of the aluminum surface is $\approx 10^{-3}$. The estimated contribution to the sky signal from the ground screen is 0.005 ± 0.004 K.

5.2.1 White Mountain

The ground at the White Mountain site is dry, rocky and rough on the scale of a wavelength. We estimate the ground to be a gray body at 273 ± 3 K with emissivity of 0.9 ± 0.1 (Ulaby *et al.* 1981) and calculate $T_{A,\text{ground}} = 0.152 \pm 0.056$ K, including emission from the ground screen.

Diffraction tests set a lower limit on $T_{A,\text{ground}}$ with the antenna pointed at the zenith. We measured a signal of 0.040 ± 0.012 K in the H-plane in the direction of highest horizon, and no signal at the ± 0.010 K level on the E-plane sides. This sets a lower limit at 0.040 ± 0.019 K, consistent with the calculation.

5.2.2 South Pole

The surface at the South Pole is smooth and flat, consisting of dry, packed ice crystals. The dielectric constant at the surface is ~1.7 and tapers smoothly to ~3.2 at depths ≥80 m. The optical depth of the ice is >100 m so that the effective ground temperature is ~225 K (the annual average temperature). Including the effect of polarized reflection from the surface and emission from the ground screen we estimate $T_{\mathrm{A,ground}} = 0.064 \pm 0.023$ K and 0.094 ± 0.034 K at 0° and 15° zenith angles, respectively. The ground emission correction is smaller at the South Pole than at White Mountain due to the lower horizon, colder ground and higher reflectivity of the surface.

5.3 INSTRUMENTAL OFFSET ΔT_{inst}

When the radiometer is inverted to observe the cold load and the zenith, its properties can change. Changes in the gain, the system temperature, the physical temperature of any lossy front-end components, and the reflection and insertion loss of each component, as well as electrical effects, can all contribute to ΔT_{inst}. The radiometer signal, S, can be written as

$$S \approx \frac{1}{G}\left[T_{\mathrm{sys}} + T_{\mathrm{A,load}}(1 - R - L) + T_{\mathrm{B}}R + T_{\mathrm{R}}L\right]$$

where the radiometer is characterized by the system temperature T_{sys}, the antenna temperature of the load $T_{\mathrm{A,load}}$, the effective reflection coefficient R, the effective insertion loss L, by the broadcast noise temperature T_{B}, and the effective physical temperature of the lossy components T_{R}. The change in output when the radiometer is inverted with a fixed load attached to the aperture is given by:

$$\begin{aligned}\Delta T_{\mathrm{inst}} = G\,\delta S \approx \delta T_{\mathrm{sys}} + \delta T_{\mathrm{B}}\,R + \delta T_{\mathrm{R}}\,L \\ - \frac{\delta G}{G}(T_{\mathrm{sys}} + T_{\mathrm{A,load}}) + \delta R\,(T_{\mathrm{B}} - T_{\mathrm{A,load}}) + \delta L\,(T_{\mathrm{R}} - T_{\mathrm{A,load}}),\end{aligned}$$

where second-order terms have been dropped in the gain-change term. The first three terms are independent of $T_{A,load}$ while the last three terms (gain, reflection, and insertion loss) are linearly dependent on $T_{A,load}$. The temperature differences in the last two terms determine the sensitivity of a particular test to δR and δL. Measurements of ΔT_{inst} at 7.5 GHz, where a cryogenic target was available, showed an effect which was linear in $T_{A,load}$ (Levin *et al.* 1992).

We needed to evaluate ΔT_{inst} for $T_{A,load} = T_{A,sky}$, but were unable to build a stable, invertible, cryogenic target of such large aperture size. We measured ΔT_{inst} by securely attaching the ambient calibration target to the antenna aperture and inverting the radiometer. Tests of the target itself showed no change in target reflection coefficient when inverted.

We performed tests at White Mountain with the load at ambient temperature (275 ± 2 K). We subsequently mounted a heater on the load; at the South Pole we measured the effect with load temperatures in the range 244 to 330 K. After returning to Berkeley, we modified the target further and performed tests with the load in the range from 223 to 331 K. Figure 4 shows the results of the tests performed with a short period (32 or 64 sec). There is no significant change from site to site, and there is no significant dependence on $T_{A,load}$. Because we lack a cryogenic measurement, the uncertainty in the effect, extrapolated to the 4 K sky temperature, becomes large. The extrapolated value is $\Delta T_{inst} = -0.009 \pm 0.061$ K.

The short period tests are insensitive to instrumental effects caused by slow thermal gradients. To measure thermal effects (*e.g.* due to changes in G), we attached the ambient temperature target to the antenna and inverted the radiometer at the 160 s period of the CMB measurement. The data, analyzed as if they were CMB measurements, showed $\Delta T_{inst} = 0.037 \pm 0.004$ K (Table 4). If this effect were due solely to gain variation, it would contribute 0.007 ± 0.001 K to the measurement. If this effect were due to any combination of variation in T_{sys}, T_B, or T_R, it would contribute 0.037 ± 0.004 K to the

CMB measurement. Since we cannot distinguish between these possibilities, we adopt the average value 0.022 ± 0.015 K for thermal effects. Added to the extrapolated value discussed previously, we obtain $\Delta T_{\mathrm{inst}} = +0.013 \pm 0.063$ K.

5.4 RF INTERFERENCE $T_{\mathrm{A,RFI}}$

Radiofrequency interference was a major factor in our choice of observation sites. We used a spectrum analyzer to search for and monitor continuous and pulsed RFI sources at both sites.

5.4.1 White Mountain

We examined the signal after the first amplifier and the 1.0–1.6 GHz bandpass filter of the radiometer. No RFI signals were observed over the bandwidth of the measurement to give an upper limit of 0.006 K due to a single spike. There was a very strong pulsed signal at 1.33 GHz which set the lower limit of our operating frequency range. The lower limit of the synthesized bandwidth was set at 1.375 GHz, giving >60 dB rejection of the source at 1.33 GHz; it contributed negligibly. Assuming 5 sources just at the limit of detectability gave a 2 σ upper limit on RFI of 0.030 K. At White Mountain in 1988, $T_{\mathrm{A,RFI}} = 0.00\ {+0.015}/{-0.000}$ K.

5.4.2 South Pole

We monitored RFI in 20 MHz bands with 1 kHz resolution over the measurement band using a separate widebeam horn and low-noise amplifier. In four of the ten bands we found only small spikes at the limit of our detection sensitivity of 5×10^{-4} K per spike. These total a maximum of ~0.005 K, or less for a duty cycle <1. In the 1.53 – 1.55 GHz band a source was observed during two of the three observations of that region. If this source were present during the measurements, the scatter on the sky data would have been of order 0.3 K, inconsistent with the observed value of 0.05 K. Some of the vehicular traffic at the Station (1.8 km away) generated pulsed noise over a wide frequency range. This was observable only when a vehicle was closer than ~0.1 km, and during observations there were no vehicles closer than 1 km. At the South Pole in 1989, $T_{A,RFI} = 0.000 +0.005/-0.000$ K.

5.5 COLD LOAD CALIBRATION $T_{A,load}$

The cold load is discussed in detail by Kogut *et al* (1990) and Bensadoun *et al.* (1992). At 1.47 GHz, approximately 99% of the signal from the cold load comes from the microwave absorber submerged in LHe. The differential pressure over the LHe bath is maintained between zero and +1 Torr during observations. At the ambient pressures of the sites, the slope of the LHe boiling point curve is ~0.0018 K/Torr (Duriex and Rusby 1983), so variations in the pressure lead to temperature variations of ~±0.001 K.

Only two sets of windows come between the radiometer and the LHe-bathed absorber. The most significant are the Fluorglas windows whose opacity near 1.47 GHz was $<2 \times 10^{-5}$; the physical temperature of these windows was ≤50 K. Two 23-μm thick polyethylene windows at the cold load aperture prevent condensation of atmospheric gases inside the load; they contribute <0.001 K to the load signal.

The total correction to the LHe bath temperature is 0.048 ± 0.023 K. Table 5 summarizes the contributions to $T_{A,Load}$. $T_{A,Load} = 3.790 \pm 0.023$ K in 1988 and 3.854 ± 0.023 K in 1989.

5.6 JOINT CONTRIBUTION $\Delta T_{A,joint}$

Differences in the joints between the horn antenna and the cold load and ground screen interface plates contributed to the observed sky-cold load temperature difference. The cold load interface plate makes the transition between the rectangular horn and the cylindrical load wall. The ground screen interface plate moves the base of the ground screen sides ~10 cm out from the edge of the antenna aperture. The contribution, $T_{A,joint}$, has three components: 1) differential emission from within the resistive metal to metal joints, 2) differential transmission (leakage) of ambient radiation through the joints, and 3) differential joint reflection. We measured the sum of the differential joint emission and transmission to be 0.016 ± 0.035 K (more signal from the ground screen joint) by comparing the signal when observing the load using the ground screen plate and the load interface plate. We made this test with the load absorber immersed in liquid nitrogen and extrapolated the test results to a LHe-temperature absorber. Because the test was not performed with a LHe-temperature absorber and the system is difficult to model, the error on this result is doubled to account for modeling errors.

We measured the difference in reflection between the antenna-ground screen interface and the antenna-load interface using a network analyzer. The reflection was slightly greater when mating with the ground screen, resulting in a 0.009 ± 0.008 K correction in the sky-cold load difference signal. The total correction is the same for the two years (the joint was unchanged): $\Delta T_{\mathrm{A,joint}} = 0.025 \pm 0.070$ K.

5.7 SOLAR EMISSION $T_{\mathrm{A,sun}}$

We avoided solar emission at White Mountain by observing only at night. At the South Pole, the sun was ~23° above the horizon. We measured the solar antenna temperature on 12 Dec 1989 to be 69 ± 5 K in beam center. During all CMB observations, the sun was >67° from beam center, reducing the antenna temperature to <0.004 K. The solar screen discussed in § 4.2 further reduced solar radiation. We adopt 0.004 K as a 68% C.L. upper limit on $T_{\mathrm{A,sun}}$.

6. THE SKY TEMPERATURE

We calculate the zenith-cold load signal difference and the gain for each CMB measurement cycle. Scatter in the differences is due to receiver noise, gain variations, and possibly from the imperfect joint at the antenna aperture (see § 5.6). The gain is stable to better than 1% over all CMB observations and varies by less than 0.2% between any two cycles. We remove the linear component of the gain drift by linear interpolation between the cold load signal of adjacent cycles. We evaluate $T_{A,sky}$ using equations (1) and (2) and the contributions evaluated in § 5. The average value of the sky temperature during each run is given in Table 6, which also summarizes all the terms entering in equations (1) and (2).

6.1 WHITE MOUNTAIN

The three runs total 51 cycles; the data from 4 cycles are discarded because of errors in the observing sequence. Figure 5 (a) shows the decreasing contribution from galactic emission in the sky temperature data as the galactic plane moves further from beam center.

6.2 SOUTH POLE

An abrupt change occurred in the zenith and cold load signals as well as a 0.13 K increase in their difference after the 18th cycle of the first set of data taken at the South Pole. Taken alone, the first part of this data set would give T_{CMB} 0.116 K lower than that given by runs 1 to 4. The latter part of the first data set is consistent with runs 1 to 4. This data set is not included in the analysis; if included, it would decrease T_{CMB} by 0.009 K.

Runs 1 to 4 have 103 cycles. Of these, we discard 7 of the high-gain data and 11 of the low-gain data points due to errors in the observing sequence. The high- and low-gain measurements of the sky temperature for each cycle agree to within the statistical errors. We use the average of the high and low gain data in the analysis. Figure 5 (b) shows data from the three runs at 15° zenith angle. An intermittent problem with a power supply caused excess noise in some of the South Pole data; this problem did not significantly change the mean zenith-cold load difference.

7. GALACTIC EMISSION $T_{A,gal}$

Emission from the galaxy is the largest correction to the zenith data and the largest source of uncertainty in the measurement. Galactic continuum emission is spatially and frequency dependent, consisting of synchrotron radiation from cosmic ray electrons and thermal electron emission (HII emission). Significant HII emission is localized near the plane of the galaxy and has a spectral index of 2.1. Synchrotron emission is characterized by a spatially and frequency dependent spectral index α.

The emission from the blend of unresolved extragalactic radio sources is small compared to galactic emission (~10% for the observed regions) and has a spectral index of ~2.75 (Willis *et al.* 1977). This emission is generally not removed from galactic radio emission maps and we include it in the galactic signal in the analysis and discussion.

We estimate the galactic signal using a 408 MHz skymap (Haslam *et al.* 1982) and a compilation of HII sources at 2.5 GHz. The 408 MHz map is first corrected for a CMB signal of 2.7 ± 1 K (which allows for the possibility of up to a 1 K spectral distortion at 408 MHz) and for HII emission (to avoid double counting). The adjusted 408 MHz skymap and the HII map are convolved with the measured antenna gain pattern to produce a profile at the declination of each observation. These profiles are then scaled to 1.47 GHz using spectral indices of 2.75 ± 0.15 for the 408 MHz data and 2.1 for the HII data. Figure 5 shows the galactic model and measured values of $T_{A,sky}$.

The accuracy of the galactic model at 1.47 GHz depends primarily on the accuracy of the 408 MHz map and the accuracy of the spectral index used to scale from 408 MHz to 1.47 GHz. The 408 MHz full-sky map, a compilation of four different surveys, has overall errors of ±3 K in the zero level and ±10% in the gain.

The largest error in the galactic signal arises from uncertainty in the spectral index. We make a first approximation of the index from the ratio of the 408 MHz map and a map at 1420 MHz (Reich and Reich, 1986), after both have been corrected for the CMB signal. For the regions observed at White Mountain this gives $\alpha \approx 2.61 \pm 0.06$ (statistical error only). In these regions, HII emission is ≤0.5% of the total emission and correcting for it would increase the result by only ~0.2%. For the entire region covered by both maps, $\delta > -19°$, $\alpha = 2.64 \pm 0.08$. The error on α due to the gain and zero level uncertainties on the maps at frequencies ν_1 and ν_2 is

$$\delta\alpha = \frac{1}{\ln\left(\nu_1/\nu_2\right)} \sqrt{\left(\frac{\delta T_1}{T_1}\right)^2 + \left(\frac{\delta T_2}{T_2}\right)^2} \tag{4}$$

where $\delta T/T$ is the relative error of the maps. In the regions observed (except WM run 1), the emission at 1420 MHz is ≤1 K, so the ±0.5 K zero level error on the 1420 MHz map dominates the uncertainty in α. For WM runs 2 and 3 the total error on α is ~±0.4.

Lawson *et al.* (1987) attempt to improve the precision in the spectral index by a better determination of the zero level of the 1420 MHz map. They assume that, for a region of low galactic emission near the North Celestial Pole, the spectral index is frequency-independent and has a value determined by the 408 MHz map and a lower frequency map at 38 MHz. They adjust the zero level of the 1420 MHz map by –0.13 K to fit the constant spectral index in the region of low emission. For WM runs 2 and 3, the Lawson-corrected maps give $\alpha \approx 2.71 \pm 0.05$ (statistical error only). The 408 MHz map introduces a ±0.13 error in α; the error introduced by the 1420 MHz map depends on the validity of the constant spectral index assumption. This procedure exploits the small (≤25%) fractional zero level errors on the 408 and 38 MHz maps in the region of minimum emission, but it relies on the assumption of a constant spectral index.

One can also estimate the spectral index by comparing differences in the galactic signal at 408 MHz and at higher frequencies. We measured the differential galactic signal at White Mountain by scanning the radiometer (mounted on the extension) ±15° from the zenith in the E-W direction. The data are plotted in Figure 6 with statistical error only. The least-squares fit to the data (also plotted in Figure 6) yields a synchrotron index $\alpha = 2.90 \pm 0.02$ (statistical error only). The low confidence level of the fit ($\chi^2 = 127$ for 27

D.O.F.) and the 0.05 K signal offset are evidence of an instrumental effect (*e.g.* radiation leakage through the joint between the antenna and extension) and/or errors in the model data. Differential galactic scans at 3.8 and 7.5 GHz at White Mountain and at 3.8 GHz at the South Pole are consistent with a synchrotron spectral index of 2.75 (see, for example, De Amici *et al.* 1991 for a plot of ±30° zenith scan data from the South Pole).

We take the spectral index of synchrotron radiation for $0.4 < \nu < 1.5$ GHz and for the regions of the sky observed to be the average of the four possible values above, 2.75, with an error of ±0.15 to include the three estimates.

The 408 MHz and HII maps are total intensity maps whereas we only measure one linearly polarized component. We use the measured polarization (Brouw and Spoelstra, 1976) of the region of sky observed at White Mountain, integrated over the main lobe of the beam, to correct the total intensity profiles.

There are no published data of the polarization for the South Celestial Pole (SCP) region, but we can use the fractional polarization at White Mountain as a guide: the largest fractional error is 7% for run 3. For a random polarization angle, we obtain 0.000 ± 0.027 K for runs 1, 2, and 4 (slightly larger for run 3). Price (1969) measures one linear polarization component of the SCP brightness at 408 MHz and observes a 0.5 K diurnal variation in the signal. He attributes the variation to differential modulation of the galactic plane by the elliptical beam. If the variation is entirely due to galactic polarization, it would scale to 0.015 K at 1.47 GHz. We adopt the larger value, 0.000 ± 0.027 K, for the South Pole.

Table 7 summarizes the sources of error in the galactic signal for the region observed during WM run 3. Other sources of error in the galactic signal are the uncertainty in the center frequency, the beam pattern, the pointing direction, and in HII emission (which we conservatively estimate at ±50%).

8. RESULTS

We remove $T_{A,gal}$ from the zenith sky temperature to obtain $T_{A,CMB}$ as summarized in Table 6. The uncertainty is dominated by systematic effects which are largely correlated from run to run and from site to site. Tables 6 and 8 indicate the correlated and uncorrelated uncertainties.

The results from the three White Mountain runs and the four South Pole runs are consistent with each other from run to run (see Table 6) to within the statistically uncorrelated part of the error. Figure 7 shows a stacked histogram of the CMB data from the combined data sets from White Mountain and from the South Pole.

The average, weighted by the statistically uncorrelated part of the error of each run, gives a CMB antenna temperature of 2.23 ± 0.25 K for the White Mountain data set and 2.23 ± 0.21 K for the South Pole data set. The error is the quadrature sum of the statistical spread in each data set and the smallest total correlated error from each data set. Converting to thermodynamic temperature, we obtain:

$$T_{CMB} = 2.27 \pm 0.25 \text{ K} \qquad \text{(White Mountain 1988)}$$

$$T_{CMB} = 2.26 \pm 0.21 \text{ K} \qquad \text{(South Pole 1989).}$$

Combining the results from the two years, weighting by the part of the error which is uncorrelated from site to site (see Table 8), we obtain:

$$T_{CMB} = 2.27 \pm 0.19 \text{ K} \qquad \text{(1988 and 1989 combined).}$$

9. DISCUSSION

9.1 COMPARISON WITH OTHER MEASUREMENTS OF THE CMB TEMPERATURE

Our result is in good agreement with the value 2.11 ± 0.38 K obtained in 1986 from the White Mountain site with an earlier version of this instrument (Levin *et al.* 1988). Including the 1986 result and weighting by the uncorrelated parts of the error (≈ 0.34 K for the 1986 result) decreases the combined result by 0.009 K. This result is consistent with $T_{CMB} = 2.8 \pm 0.6$ K at 1.45 GHz measured by Howell and Shakeshaft (1966).

The CMB result is 0.47 K, or 2.5 σ (~1% probability), below the 2.74 ± 0.01 K global average (the weighted mean of all CMB measurements). Other low-frequency ground-based measurements have reported CMB temperatures systematically lower than the global average; however none deviate by as much as the present result. This disagreement is due either to an undetected problem with the measurement or a distortion in the CMB spectrum, or both.

9.2 POTENTIAL SOURCES OF ERROR

The errors in the measurement are summarized in Tables 7 and 8. If the deviation from the global average is due to a problem with the cold load, the additional emission would be many times the 0.05 K total correction to the absorber temperature.

Sources of scatter in the sky-cold load differences, such as ΔT_{inst}, $\Delta T_{\mathrm{A,joint}}$ and gain variations, could have changed during the 10-day observation and testing period. However, values of $T_{\mathrm{A,sky}}$ in a region observed during three of the South Pole runs are in excellent agreement. For the overlapping interval, $4.1^{\mathrm{h}} < \mathrm{RA} < 4.7^{\mathrm{h}}$, the mean and standard deviation in the mean of $T_{\mathrm{A,sky}}$ is 2.776 ± 0.016 K, 2.773 ± 0.029 K, and 2.781 ± 0.022 K for runs 1, 2, and 4, respectively. The corrections to these subsets of data are the same over this interval. The agreement suggests that the sum of ΔT_{inst}, $\Delta T_{\mathrm{A,joint}}$, $T_{\mathrm{A,sun}}$, $T_{\mathrm{A,RFI}}$ and the effect of gain variations (contributions which were not *a priori* known to be constant) was constant at the ~0.01 K level.

Our estimate of ΔT_{inst} is based on measurements with load temperatures in the range 223 to 331 K. We are unable to measure the dependence of ΔT_{inst} for load temperatures closer to 4 K; such measurements could have changed our estimate of ΔT_{inst}.

We rely on the theoretical understanding of atmospheric microwave emission to extrapolate the 7.5 and 3.8 GHz $T_{\mathrm{A,atm}}$ measurements to 1.47 GHz. If the roll-off in atmospheric emission occurs closer to 1.47 GHz than predicted by theory, then the atmospheric contribution has been overestimated (see § 5). The data from the two sites are insensitive to the roll-off frequency. If the 7.5 and 3.8 GHz measurements both overestimate the atmospheric temperature by 0.1 K, the extrapolated $T_{\mathrm{A,atm}}$ at 1.47 GHz would be ~0.09 K too high and T_{CMB} ~0.09 K too low.

Galactic emission may have been overestimated although the small (~0.57 K) emission at the South Pole makes overestimate of the galactic signal an unlikely source of the entire deviation. The zero level of the 408 MHz map would have to be decreased by 12 K to raise the result by $2\ \sigma = 0.38$ K. The gain of the 408 MHz map would have to be 63% lower, or the spectral index 0.77 higher, to raise the result by $2\ \sigma$.

If the disagreement with the global average is due to measurement error, it is likely due to several of the above sources.

We have repeated this measurement from the South Pole site in December 1991. We made an improved measurement of ΔT_{inst} and modified the joint at the antenna aperture to eliminate the sources of uncertainty in $\Delta T_{\mathrm{A,joint}}$. The magnitude and error of the ground signal was reduced and improvements were made to the cold load. Preliminary analysis indicates no significant undetected errors in the 1988 and 1989 data. Further analysis of the data, including 1.47 GHz atmospheric emission data, is in progress. We also made measurements at nearby frequencies which will aid in the removal of the galactic and atmospheric signals. We are planning a direct measurement of the cold load wall emission.

9.3 FITS TO CMB DISTORTION MODELS

Table 9 lists data from recent CMB measurements. These data are plotted in Figure 8 with the largest chemical potential and free-free distortions allowed at the $2\ \sigma$ level. These fits are to all of the recent data as well as pre-1980 measurements (see Weiss, 1980). The best-fit Planck spectrum is for $T_{\mathrm{CMB}} = 2.738 \pm 0.008$ K ($1\ \sigma$ error) with $\chi^2/\mathrm{DOF} = 44/47$. The best-fit chemical potential distortion for $\Omega_b = 0.05$ is for an unperturbed CMB temperature $T_{\mathrm{CMB}} = 2.748 \pm 0.013$ K and $\mu = (2.3 \pm 1.2) \times 10^{-3}$ ($1\ \sigma$

error) with χ^2/DOF = 35/46. The best-fit free-free distortion for $\Omega_b = 0.05$ is for Y_{ff} = (–1.0 ± 2.4) x 10^{-5} (1 σ error) with χ^2/DOF = 43/46.

The significance of the best-fit μ and Y_{ff} values increases with this result because it lies significantly below the high-frequency mean. The 1.47 GHz data point adds ~2 to the χ^2 of the μ-distorted spectra fits and adds 6-7 for the Y_{ff}-distorted spectra and the Planck fits indicating that the new point makes either distortion a worse fit to the data. This is because the low frequency results (ν < 10 GHz) are lower than the results at ν > 30 GHz and the distorted spectra do not have enough curvature in the 10 < ν < 30 GHz region to dip down fast enough.

The fits to $T_{\rm CMB}$ data require comparison of data from different experiments with different galactic corrections. At low frequencies, the galactic corrections are large and the CMB data have much larger uncertainties than the measured sky brightness. An alternate approach is to use only our own White Mountain data and examine the frequency dependence of the sky brightness. Since the spectral index of galactic synchrotron emission is fairly well known, this exploits the precise sky brightness data to search for CMB distortions.

For the sky brightness fits we assume only the spectral index of galactic emission, α = 2.75 ± 0.15, and fit to Planck, μ-, and Y_{ff}-distorted CMB spectra. We fit to antenna temperature data in the direction $1.5^{\rm h}$ RA, 38° dec (l=132°, b=–24°) at 1.47, 2.5, 3.8, 4.75, 7.5, 10, 33, and 90 GHz. This procedure assumes the measurements were made with similar beams, however the direction is far enough from the galactic plane so that the error due to unequal beamwidths is small. The error is largest at low frequency: the 2.5 GHz datum would increase by <0.02 K (<10% of the error on the datum) if the beam were as large as that at 1.47 GHz. The measurements are of brightness in one linear polarization (not necessarily the same orientation for each datum). The potential error is largest at low frequency. For these fits, we make a +0.06 K polarization correction to $T_{\rm A,sky}$ at 1.47 GHz (see § 7). We do not apply a polarization correction to the higher frequency data. The error due to galactic polarization is ~±0.03 K at 2.5 GHz and less at higher frequency.

The best-fit is for $T_{\mathrm{A,gal}}(1.47 \text{ GHz}) \approx 0.45$ K, with an uncertainty of ±0.14 to ±0.22 K, depending on the CMB spectrum. This is 0.36 ± 0.31 lower than the value obtained by scaling the 408 MHz survey by $\alpha = 2.75$. Part of this difference can be explained by the overall average of the data set which is ~0.10 K lower than the global average T_{CMB} (the best-fit T_{CMB} is 2.622 to 2.633 K with 1 σ errors of ~±0.033 for Planck and Y_{ff}-distorted CMB spectra and ±0.067 K for a μ-distorted spectrum).

For the sky brightness fits, the best-fit chemical-potential distorted spectrum is for μ ~$(0 \pm 3.5) \times 10^{-3}$ (1 σ error) with χ^2/DOF = 3.5/5. The best-fit free-free distorted spectrum is for Y_{ff} ~$(-1.0 \pm 2.6) \times 10^{-5}$ (1 σ error) with χ^2/DOF = 3.4/5. Fits to our White Mountain data set determine the CMB temperature and yield spectral information. Although not as precise as the limits set by fits to the full data set, the results of these fits are independent of the magnitude of galactic emission, the largest source of error in low-frequency measurements.

9.4 COMPARISON WITH OTHER LOW-FREQUENCY SKY BRIGHTNESS MEASUREMENTS

The precision of the spectral index of sky brightness (and therefore galactic emission) as calculated from pairs of measurements is due to the gain and zero-level errors of those measurements. Our result at 1.47 GHz is near the 1.42 GHz survey of Reich and Reich (1982) and can serve to recalibrate that and other low-frequency surveys.

The absolute zero level of the 1420 MHz survey is determined by comparison with the absolutely calibrated data of Howell and Shakeshaft (1966) and Pelyushenko and Stankevich (1969). The latter measurement should not be used due to "improper treatment of the instrument output" (Danese and De Zotti, 1988). Large uncertainties in the measurement of Howell and Shakeshaft arise from the cold load calibration (the LHe-cooled coaxial termination contributes ±0.2 K uncertainty), the correction for near-sea-level atmospheric emission (±0.2 K uncertainty), and the calculated correction for antenna loss (±0.2 K uncertainty).

We fit the sky-brightness spectrum to the total-intensity sky surveys at 408, 820 and 1420 MHz and the 1.47 GHz total-intensity sky brightness datum. Assuming a CMB spectrum obtained by a least-squares fit to the entire CMB data set, we calculate the best-fit (constant) galactic spectral index. The best-fit spectral index is 3.1±0.2 for a Planck spectrum (χ^2/DOF ~ 10/2). Assuming a μ- or Y_{ff}-distorted spectrum does not change the result significantly. This spectral index is ~1.5 σ higher than the value used to calculate galactic emission in § 7. This is evidence that the measured sky brightness at 1.47 GHz is low or the others are high.

If we assume that the difference between the best-fit sky brightness (with amplitude and spectral index of galactic emission as free parameters) and the data are due to zero-level errors in the data, then we obtain zero level corrections to the data. The residuals are +3.0, −1.9, −0.41, and +0.22 K at 0.408, 0.820, 1.42, and 1.47 GHz, respectively, where we have assumed a Planckian CMB. Assuming a μ- or Y_{ff}-distorted spectrum does not change the residuals significantly.

10. CONCLUSIONS

We have measured $T_{\rm CMB}$ = 2.27 ± 0.19 K from high altitude sites at White Mountain and the South Pole. Changes in the ground, atmospheric, galactic and solar contributions, as well as different RFI at the two sites indicate that ~±0.13 K of the errors in the two measurements are uncorrelated; the results agree to 0.01 K.

The major source of error in the CMB measurement is due to Galactic emission. The error in the sky brightness measurement is due to approximately equal contributions from the corrections for atmospheric and ground emission, antenna aperture joint effects, and changes in the instrument offset.

The entire CMB spectrum data set is consistent with zero free-free distortion. The entire CMB spectrum data set is best fit by a chemical-potential-distorted CMB spectrum which is only marginally consistent with a Planck spectrum. However, the non-zero chemical-potential distortion may be due entirely to the ~0.1 K difference in the averages of the White Mountain and high-frequency data sets which mimics a spectrum which dips at low frequencies .

The set of White Mountain sky brightness data (the sum of galactic and CMB emission) is consistent with a Planck CMB spectrum.

Fits to the White Mountain data set and to the low-frequency surveys indicate that the new datum is too low by ~0.2 K $\approx$ 1 σ, but not by 0.5 K. This may be due to a zero-level error in the measurement and/or our understanding of the galaxy. Zero-level error in the measurement may be due to the cold load calibration, the corrections for galactic and atmospheric emission, and instrumental effects.

11. ACKNOWLEDGEMENTS

We thank the staffs and crews of the White Mountain Research Station and of the Amundsen-Scott South Pole Research Station, and the staffs at ITT Antarctic Services and at the NSF Division of Polar Programs. We also gratefully acknowledge the assistance of John Gibson, Tap Lum, Jon Aymon, Giuseppe Bonelli, Francesco Cavaliere, Barron Chugg, Gary Hinshaw, Jenny Hwang, Christine Ing, Richard Kuiper, Jay Levin, Larry Levin, Armando Meuti, Faye Mitschang, and Giorgio Sironi for their help with various parts of this research. M. Bersanelli acknowledges support from ENEA, Progetto Antartide; M. Limon acknowledges support from Fondazione Angelo Della Riccia. This research was funded in part by the National Science Foundation Grants Numbers DPP 8716548 and AST 8406187 and by the Director, Office of Energy Research, Office of High Energy and Nuclear Physics, Division of High Energy Physics of the U.S. Department of Energy under Contract DE-AC03-76SF00098.

REFERENCES

Bartlett, J. and Stebbins, A., 1991, Ap. J., 371, 8.

Bensadoun M., *et al.*, 1992, *Rev. Sci. Inst.,* submitted.

Brouw, W. N., Spoelstra, T. A. Th., 1976, *Astron. Astophys. Suppl.*, **26**, 129.

Burigana, C., Danese, L. and De Zotti, G., 1991, *Astron. Astroph.,* **246**, 49.

Danese, L. and Partridge, R.B., 1989, *Ap. J.*, **342**, 604.

De Amici, G., *et al.*, 1991, *Ap. J.*, **381**, 341.

De Amici, G., *et al.*, 1990, *Ap. J.*, **359**, 219.

Duriex, M. and Rusby, R.L., 1983, *Metrologia*, **19**, 67.

Gordon, R. G., 1967, *J. Chem. Phys.*, **46**, 448.

Haslam, C.G.T., Salter, C.J., Stoffel, H., and Wilson, W.E., 1982, *Astr. Astroph. Suppl. Ser.*, **47**, 1.

Howell, T.F., and Shakeshaft, J.R., 1966, *Nature*, **210**, 1318.

Kogut, A., *et al.*, 1990, *Ap. J.*, **355**, 102.

Kogut, A., *et al.*, 1991, in: Holt, S., Bennet, C., and Trimble, V. (edts.), AIP Conf. Proc. 222: After the First Three Minutes, (AIP: New York) p 62.

Lawson, K. D., *et al.*, 1987, *Mon. Not. R. astr. Soc.*, **225**, 307.

Levin, S.M., *et al.*, 1988, *Ap. J.*, **334**, 14.

Levin, S.M., *et al.*, 1992, *Ap. J.*, **396**, in press.

Mather, J., *et al.*, 1990, *Ap.J. Lett.*, **354**, L37.

Pauliny-Toth, I.I.K., and Shakeshaft, J.R., 1962, *Mon. Not. R. astr. Soc.*, **124**, 61.

Pelyushenko and Stankevich 1969, *Sov. Astron.*, **13**, 223.

Price, R.M., 1969, *Aust. J. Phys.*, **22**, 641.

Reich, P., and Reich, W., 1986, *Astr. Astroph. Suppl. Ser.*, **63**, 205.

Silk, J. and Stebbins, A., 1983, *Ap.J.*, **269**, 1.

Sironi, G., *et al.*, 1991, *Ap.J.* , **378**, 550.

Sironi, G., *et al.*, 1992, *Ap.J. Lett.*, submitted.

Smoot, G., *et al.*, 1983, *Phys. Rev. Lett.*, **51**, 1099.

Ulaby, F.T., Moore, R.K., Fung, A.K., 1981, Microwave Remote Sensing: Active and Passive, Vol. 1, (Addison-Wesley Publishing Company, Reading, MA)

Weiss, R. 1980, *Ann. Rev. Astron. Astrophy.*, **18**, 489.

Willis, A. G., et al., 1977, in: IAU Symp. No. 74, Radio Astronomy and Cosmology, pg. 39, Jauncey, D. L. ed., D. Reidel, Dordrecht, Holland.

Witebsky, C., *et al.*, 1987, *IEEE Trans. Antennas Propagat.,* **AP-35**, 1310

TABLE 1

1.5 GHZ RADIOMETER PARAMETERS

Parameter	Value	Comments
Center frequency	1.47 ± 0.01 GHz	Measured ($\lambda = 20.4$ cm)
YIG filter bandwidth	26 MHz	Measured
YIG sweep rate	1 GHz/sec	Measured
Synthesized bandwidth	200 MHz	Measured
System temperature	53.5 ± 0.4 K[a]	Measured with cold and warm loads
Sensitivity	10 mK $Hz^{-1/2}$	Theoretical
	18 mK $Hz^{-1/2}$	Measured
Beamwidth (HPBW)	30° x 27°	ExH-plane, measured w/ ground screen
Beam area	0.284 sr	Calculated
low gain	25.0 ± 0.2 K/V	WM, measured
	24.2 ± 0.1 K/V	SP, measured
gain ratio	2.537 ± 0.025	WM, measured
	2.488 ± 0.005	SP, measured
high gain	9.84 ± 0.12 K/V	WM, calculated
	9.74 ± 0.05 K/V	SP, calculated
DC amplifier offset	−10.04 ± 0.04 V	Measured with terminated input

[a] Uncertainty is the quadrature sum of the spread in measured values and the error on each value

TABLE 2

ATMOSPHERIC TEMPERATURE $T_{\mathrm{A,Atm}}(z)$ AT 1.47 GHZ

Quantity	White Mountain	South Pole		Units
zenith angle z	0	0	15	deg
7.5 GHz datum extrapolated	0.894±0.061[a]	0.979±0.067[a]		K
3.8 GHz datum extrapolated	0.846±0.063[a]	0.966±0.069[a]		K
weighted mean	0.871±0.062[a]	0.973±0.068[a]		K
$\langle f(z) \rangle$	1.071±0.022	1.071±0.022	1.114±0.024	
$T_{\mathrm{A,Atm}}(z)$	0.932±0.070	1.041±0.076	1.083±0.079	K

[a] pencil-beam intensity

TABLE 3

ESTIMATED GROUND CONTRIBUTION FOR THE ANTENNA WITH GROUND SCREEN (K)

z (deg)	White Mountain	South Pole
0	0.147 ± 0.056	0.059 ± 0.023
15	···	0.089 ± 0.034

TABLE 4

RESULTS OF 160 S PERIOD ΔT_{inst} TESTS

Test Location	Number of cycles	$T_{\mathrm{A,load}}$ (K)	Effect (K)
WM	10	275 ± 2	0.045 ± 0.012
SP	12	244 ± 5	0.035 ± 0.006
SP	6	246 ± 5	–0.026 ± 0.032
SP	10	251 ± 5	0.041 ± 0.008
			0.037 ± 0.004[a]

[a] Weighted mean and statistical error in the mean; rms = 0.033 K

TABLE 5

COLD LOAD TEMPERATURE (K)

Quantity	White Mountain	South Pole
Barometric pressure (Torr)	485	520
T_{Absorber} [a]	3.777 ± 0.002	3.842 ± 0.002
$T_{\mathrm{A,\,Absorber}}$	3.742 ± 0.002	3.806 ± 0.002
Radiometric wall emission[b]	0.024 ± 0.016	
Window emission	0.001 ± 0.001	
Incoherent reflection	0.023 ± 0.015	
Coherent reflection	0.000 ± 0.008	
Total correction to $T_{\mathrm{A,Absorber}}$	0.048 ± 0.023	
$T_{\mathrm{A,Load}}$	3.790 ± 0.023	3.854 ± 0.023

[a] T_{LHe} data from Duriex and Rusby, 1983

[b] The corrections to $T_{\mathrm{A,Absorber}}$ are the same in the two years

TABLE 6 SUMMARY OF WHITE MOUNTAIN AND SOUTH POLE SKY AND CMB DATA ANALYSIS

Quantity	WM run 1	WM run 2	WM run 3	SP run 1	SP run 2	SP run 3	SP run 4
Time (UT)	19 Sep 4:47-5:33	19 Sep 6:16-6:57	19 Sep 8:58-9:54	17 Dec 5:02-7:00	18 Dec 4:40-5:43	18 Dec 8:02-8:46	19 Dec 4:36-5:40
RA (h)	20.8-21.9	22.3-23.0	1.0-1.9	4.1-6.0	3.7-4.7	7.1-7.7	3.7-4.7
Zenith angle (deg)	0	0	0	15	15	0	15
No. of data points	16	11	19	43	22	14	23
$G(S_{\rm zenith}$-$S_{\rm load})$[a,b]	1.100±0.027	0.546±0.012	0.434±0.008	0.178±0.009	0.145±0.022	0.391±0.010	0.152±0.016
$T_{\rm A,load}$	3.790±0.023	3.790±0.023	3.790±0.023	3.854±0.023	3.854±0.023	3.854±0.023	3.854±0.023
$\Delta T_{\rm rad}$	0.013±0.063	0.013±0.063	0.013±0.063	0.013±0.063	0.013±0.063	0.013±0.063	0.013±0.063
$\Delta T_{\rm A,joint}$	0.025±0.072	0.025±0.070	0.025±0.070	0.025±0.070	0.025±0.070	0.025±0.070	0.025±0.070
$T_{\rm A,zenith}$[c]	4.852±0.102	4.298±0.098	4.186±0.097	3.994±0.097	3.961±0.100	4.207±0.097	3.968±0.098
$T_{\rm A,atm}$	0.932±0.070	0.932±0.070	0.932±0.070	1.083±0.079	1.083±0.079	1.041±0.076	1.083±0.079
$T_{\rm A,ground}$	0.152±0.056	0.152±0.056	0.152±0.056	0.094±0.034	0.094±0.034	0.064±0.023	0.094±0.034
$T_{\rm A,sun}$	0.000±0.000	0.000±0.000	0.000±0.000	0.000±0.004	0.000±0.004	0.000±0.004	0.000±0.004
$T_{\rm A,RFI}$	0.000±0.015	0.000±0.015	0.000±0.015	0.000±0.005	0.000±0.005	0.000±0.005	0.000±0.005
$T_{\rm A,sky}$[a,c,d]	3.768±0.028 ±0.137	3.214±0.014 ±0.133	3.102±0.011 ±0.133	2.817±0.012 ±0.131	2.784±0.023 ±0.132	3.102±0.010 ±0.126	2.791±0.016 ±0.131
$T_{\rm A,gal}$[a,c,d]	1.498±0.150 ±0.317	0.990±0.069 ±0.223	0.866±0.063 ±0.219	0.583±0.015 ±0.162	0.569±0.015 ±0.160	0.819±0.058 ±0.205	0.573±0.015 ±0.161
$T_{\rm A,CMB}$[d]	2.269±0.152 ±0.346	2.224±0.070 ±0.269	2.236±0.064 ±0.257	2.234±0.018 ±0.208	2.215±0.027 ±0.207	2.282±0.059 ±0.241	2.218±0.022 ±0.207

[a] Average value during run

[b] Statistical error only; includes correction for atmospheric absorption

[c] Component polarized along lines of constant RA (towards the NCP for WM data; in the direction of the indicated RA for the SP data)

[d] The first entry is the error which is statistically uncorrelated from run to run (see Table 8); the second entry is the total error

TABLE 7

SOURCES OF ERROR IN THE MODELED GALACTIC SIGNAL (K) [a]

Source	Uncertainty in Source	Error at 1.47 GHz
CMB correction to 408 MHz map	± 1 K	± 0.029
408 MHz map zero level	± 3 K	± 0.088
408 MHz map gain	± 10%	± 0.079
Spectral index	± 0.15	± 0.151
Polarized emission	± 10° angle, ± 0.03 K intensity	± 0.033
Beam pattern	± 2° angle, ± 1 dB gain	± 0.020
Center frequency	± 5 MHz	± 0.015
Pointing	± 2°	± 0.053
HII emission	± 50%	± 0.002
Total (added in quadrature)		± 0.205

[a] Calculated for 24 K total galactic emission at 408 MHz, and 0.01 HII emission at 1.47 GHz (signals during WM run 3); see text for an explanation of the uncertainties.

TABLE 8

STATISTICAL INDEPENDENCE OF ERRORS IN THE MEASUREMENTS (K) [a]

Source of error	WM Run 3			SP Run 4		
	Total error	uncorrelated error run-run	uncorrelated error site-site	Total error	uncorrelated error run-run	uncorrelated error site-site
$G(S_{\mathrm{zenith}}-S_{\mathrm{load}})$[a]	0.008	0.008	0.008	0.016	0.016	0.016
$T_{\mathrm{A,load}}$	0.023	0.002	0.002	0.023	0.002	0.002
ΔT_{inst}	0.063	0[b]	0.011	0.063	0	0.011
$\Delta T_{\mathrm{A,joint}}$	0.070	0	0.035	0.070	0	0.035
$T_{\mathrm{A,atm}}$	0.070	0	0.049	0.079	0	0.063
$T_{\mathrm{A,ground}}$	0.056	0	0.032	0.034	0	0.010
$T_{\mathrm{A,sun}}$	0.000	0	0	0.004	0	0.004
$T_{\mathrm{A,RFI}}$	0.015	0.007	0.015	0.005	0.002	0.005
$T_{\mathrm{A,gal}}$[c]	0.219	0.063	0.129	0.161	0.015	0.092
CMB correction to 408 MHz map	0.029	0	0	0.029	0	0
408 MHz map zero level	0.088	0	0.029	0.088	0	0.029
408 MHz map gain	0.086	0.020	0.043	0.057	0	0.040
Spectral index	0.166	0.045	0.100	0.109	0	0.066
Polarization	0.033	0.030	0.033	0.027	0	0.027
Beam pattern	0.020	0	0	0.020	0	0
Center frequency	0.016	0	0	0.011	0	0
Pointing	0.053	0.026	0.053	0.030	0.015	0.030
HII emission	0.002	0.002	0.002	0.003	0	0.003
Total site-site uncorrelated error for all runs at each site:[d]		0.140 (WM)			0.116 (SP)	

[a] The error breakdown is given for one of the runs at each site.

[b] A zero entry indicates that we take none of the error to be uncorrelated.

[c] The sources of uncorrelated error in the galactic signal are given; values represent the average during the run.

[d] The uncorrelated error in each averaged result is less than that for the individual runs.

TABLE 9. CMB RESULTS SINCE 1980 [a]

ν [GHz]	λ [cm]	T_{CMB} [K]	Sigma [K]	Technique[b]	Reference
0.6	50	3.0	±1.2	Ground (Term)	Sironi *et al.* 1990, *Ap.J.*, **357**, 301.
0.820	36.6	2.7	±1.6	Ground (Term)	Sironi *et al.* 1991, *Ap. J.*, **378**, 550.
1.410	21.26	2.11	±0.38	Ground (CL)	Levin *et al.* 1988, *Ap.J.*, **334**, 14.
1.47	20.4	2.27	±0.19	Ground (CL)	Bensadoun *et al.*, (this work)
2.5	12	2.79	±0.15	Ground (CL)	Sironi & Bonelli 1986, *Ap.J.*, **311**, 418.
2.5	12	2.50	±0.34	Ground (CL)	Sironi et al. 1991, *Ap. J.*, **378**, 550.
3.8	7.9	2.64	±0.07	Ground (CL)	De Amici et al. 1990, *Ap.J.*, **359**, 219.
4.75	6.3	2.70	±0.07	Ground (CL)	Mandolesi et al. 1986, *Ap.J.*, **310**, 561.
7.5	4.0	2.64	±0.06	Ground (CL)	Levin *et al.* 1992, *Ap.J.*, **396**, in press.
10	3.0	2.62	±0.06	Ground (CL)	Kogut et al. 1990, *Ap.J.*, **355**, 102.
24.8	1.2	2.783	±0.025	Balloon	Johnson & Wilkinson 1987, *Ap.J. Lett.*, **313**, L1.
33.0	0.909	2.81	±0.12	Ground (CL)	De Amici et al. 1985, *Ap.J.*, **298**, 710.
90	0.33	2.60	±0.09	Ground (CL)	Bersanelli et al. 1989, *Ap.J.*, **339**, 632.
90.3	0.332	<2.97		Balloon	Bernstein et al. 1990, *Ap.J.*, **362**, 107.
113.6	0.264	2.70	±0.04	CN (ζ Per)	Meyer & Jura 1985, *Ap.J.*, **297**, 119.
113.6	0.264	2.74	±0.05	CN (ζ Oph)	Crane et al. 1986, *Ap.J.*, **309**, 822.
113.6	0.264	2.76	±0.07	CN (HD 21483)	Meyer et al. 1989, *Ap.J. Lett.*, **343**, L1.
113.6	0.264	2.796	+0.014/-0.039	CN (ζ Oph)	Crane et al. 1989, *Ap.J.*, **346**, 136.
113.6	0.264	2.75	±0.04	CN (ζ Per)	Kaiser & Wright 1990, *Ap.J. Lett.*, **356**, L1.
113.6	0.264	2.834	±0.085	CN (HD 154368)	Palazzi et al. 1990, *Ap.J.*, **357**, 14.
154.8	0.194	<3.02		Balloon	Bernstein et al. 1990, *Ap.J.*, **362**, 107.
195.0	0.154	<2.91		Balloon	Bernstein et al. 1990, *Ap.J.*, **362**, 107.
227.3	0.132	2.76	±0.20	CN (ζ Per)	Meyer & Jura 1985, *Ap.J.*, **297**, 119.
227.3	0.132	2.75	+0.24/-0.29	CN (ζ Oph)	Crane et al. 1986, *Ap.J.*, **309**, 822.
227.3	0.132	2.83	±0.09	CN (HD 21483)	Meyer et al. 1989, *Ap.J. Lett.*, **343**, L1.
227.3	0.132	2.832	±0.072	CN (HD 154368)	Palazzi et al. 1990, *Ap.J.*, **357**, 14.
266.4	0.113	<2.88		Balloon	Bernstein et al. 1990, *Ap.J.*, **362**, 107.
30-600	1.0–0.05	2.735	±0.06	Satellite (FIRAS)	Mather et al. 1990, *Ap.J. Lett.*, **354**, L37.
30-600	1.0–0.05	2.736	±0.017	Rocket (COBRA)	Gush et al. 1990, *Phys. Rev. Lett.*, **65**, 537.

[a] Data are plotted in Figure 8

[b] Ground-based experiments calibrating with a LHe-cooled coaxial termination (Term) or a quasi-free space LHe-cooled load (CL) are indicated. For cyanogen (CN) measurements we report in parentheses the observed star.

FIGURE CAPTIONS

Figure 1. Block diagram of the 1.47 GHz radiometer. Amplifier gains and attenuator values are shown.

Figure 2. Atmospheric antenna temperature for a pencil beam. Measured data at 3.8 and 7.5 GHz from WM (open circles) and SP (open squares); extrapolated values for WM (filled circle) and SP (filled square). Two atmospheric models for WM (two lower curves) and for the SP (two upper curves) are plotted. The solid lines are the best-fit extrapolation from the measured data according to the model described by equation (3). For comparison, the model of Danese and Partridge is shown with dashed lines. The data have been corrected for the finite beamwidth of each instrument.

Figure 3. Measured E- and H-Plane gain pattern. Data taken with the ground screen on the radiometer antenna.

Figure 4. $\Delta T_{\rm inst}$ versus $T_{\rm A,load}$ for tests done at WM (triangles), the SP (squares), and Berkeley (open circles). The least-squares fit line is drawn with the filled circle is the effect at $T_{\rm A,load} = 4$ K (see text for discussion of the error).

Figure 5. Measured antenna temperature of the sky ($= T_{\rm A,CMB} + T_{\rm A,gal}$), and the predicted galactic signal (see § 7). Each data point is the sky temperature computed from one zenith-cold load comparison measurement. Representative total error bars are shown for the measured data. The three error bars shown at the left on the galactic profiles are (l. to r.) estimates of the total galactic error, the part of the error which is independent from site to site, and that part which is independent from run to run. (a) All WM data at 38° dec. (b) SP runs at –75° dec.

Figure 6. ±15° galactic zenith scan data and model. The data is shown with statistical error bars only. The solid line is the profile predicted from the model discussed in the text. The dotted line is the result of a least-squares fit with the synchrotron spectral index (best-fit value = 2.90), the vertical offset (+0.050 K) and the horizontal offset (–4°) as free parameters.

Figure 7. Stacked histogram of combined White Mountain and combined South Pole CMB data.

Figure 8. CMB results obtained since 1980 divided according to the measurement technique. Superimposed on the data are the best-fit Planck spectrum (dotted line), and the largest chemical potential (solid line) and free-free (dashed line) distortions allowed by the data at the 95% confidence level (see text).

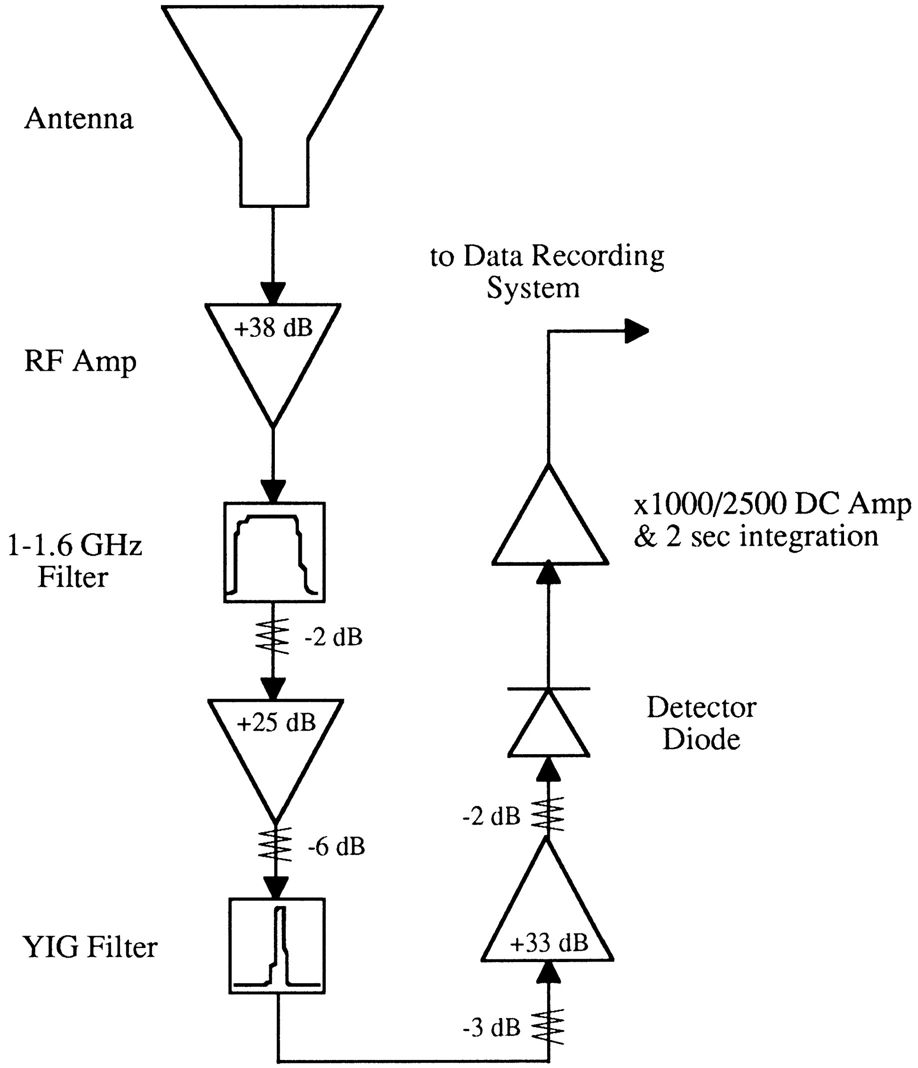
Antenna
RF Amp
+38 dB
1-1.6 GHz Filter
-2 dB
+25 dB
-6 dB
YIG Filter
-3 dB
+33 dB
-2 dB
Detector Diode
x1000/2500 DC Amp & 2 sec integration
to Data Recording System

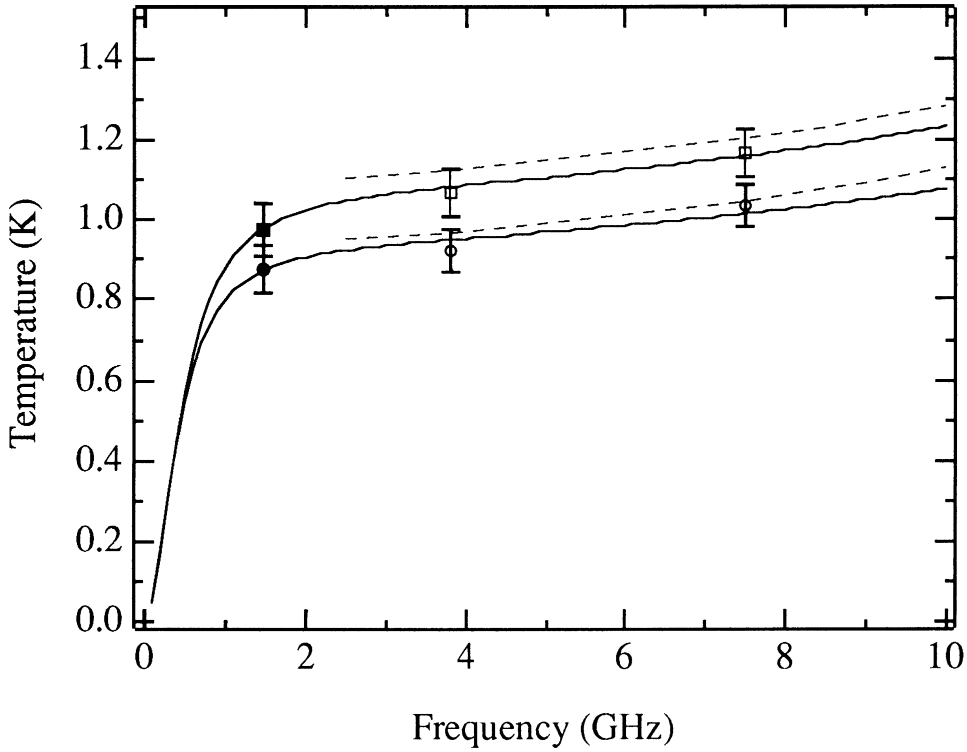
Temperature (K)
Frequency (GHz)
0.0
0.2
0.4
0.6
0.8
1.0
1.2
1.4
0
2
4
6
8
10

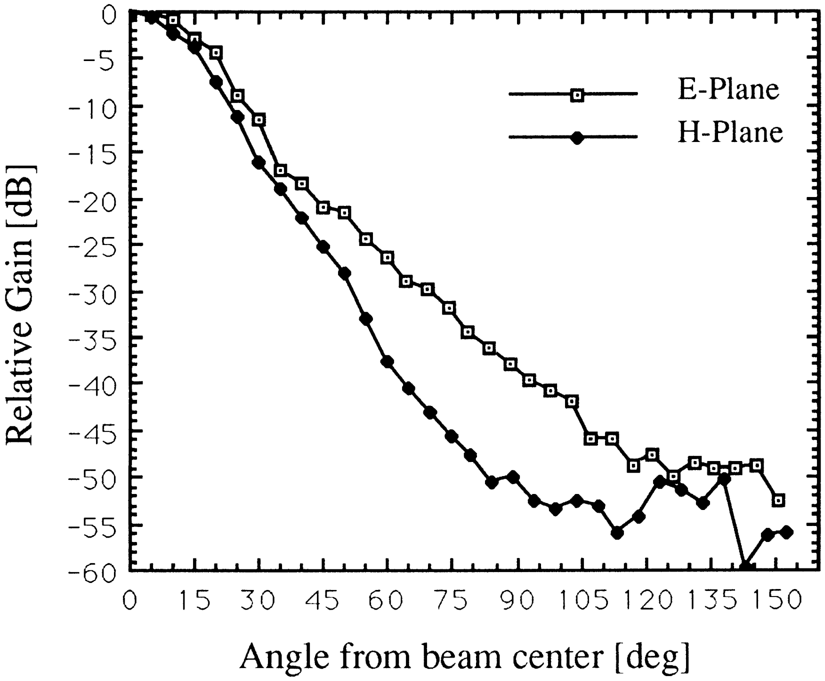
E-Plane
H-Plane
Relative Gain [dB]
0
-5
-10
-15
-20
-25
-30
-35
-40
-45
-50
-55
-60
0
15
30
45
60
75
90
105
120
135
150
Angle from beam center [deg]

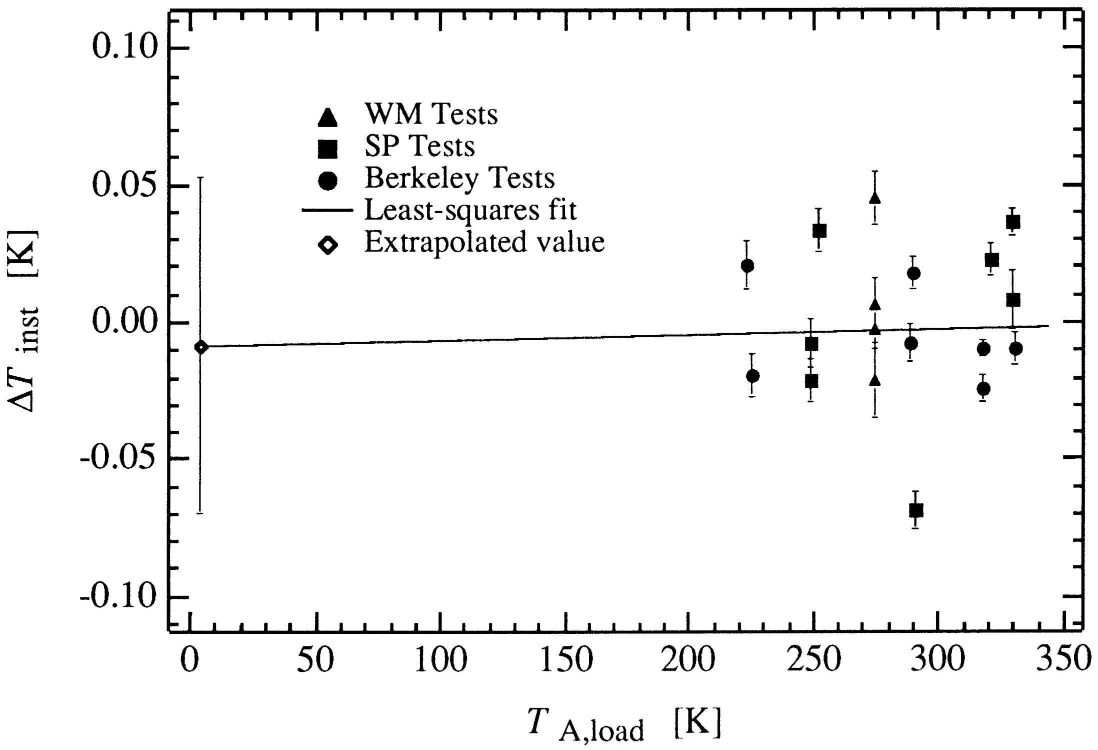

WM Tests
SP Tests
Berkeley Tests
Least-squares fit
Extrapolated value
0.10
0.05
0.00
-0.05
-0.10
ΔT_{inst} [K]
0
50
100
150
200
250
300
350
$T_{\mathrm{A,load}}$ [K]

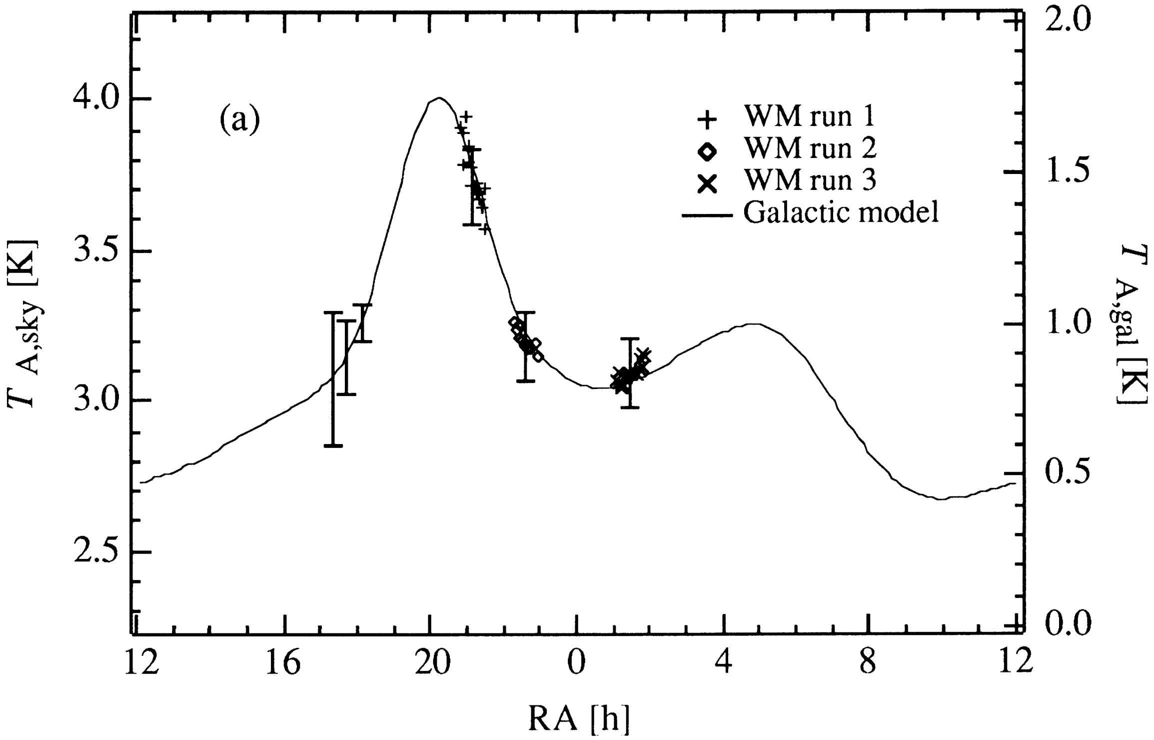
(a)
+ WM run 1
◇ WM run 2
× WM run 3
— Galactic model
$T_{\mathrm{A,sky}}$ [K]
$T_{\mathrm{A,gal}}$ [K]
RA [h]
4.0
3.5
3.0
2.5
2.0
1.5
1.0
0.5
0.0
12
16
20
0
4
8
12

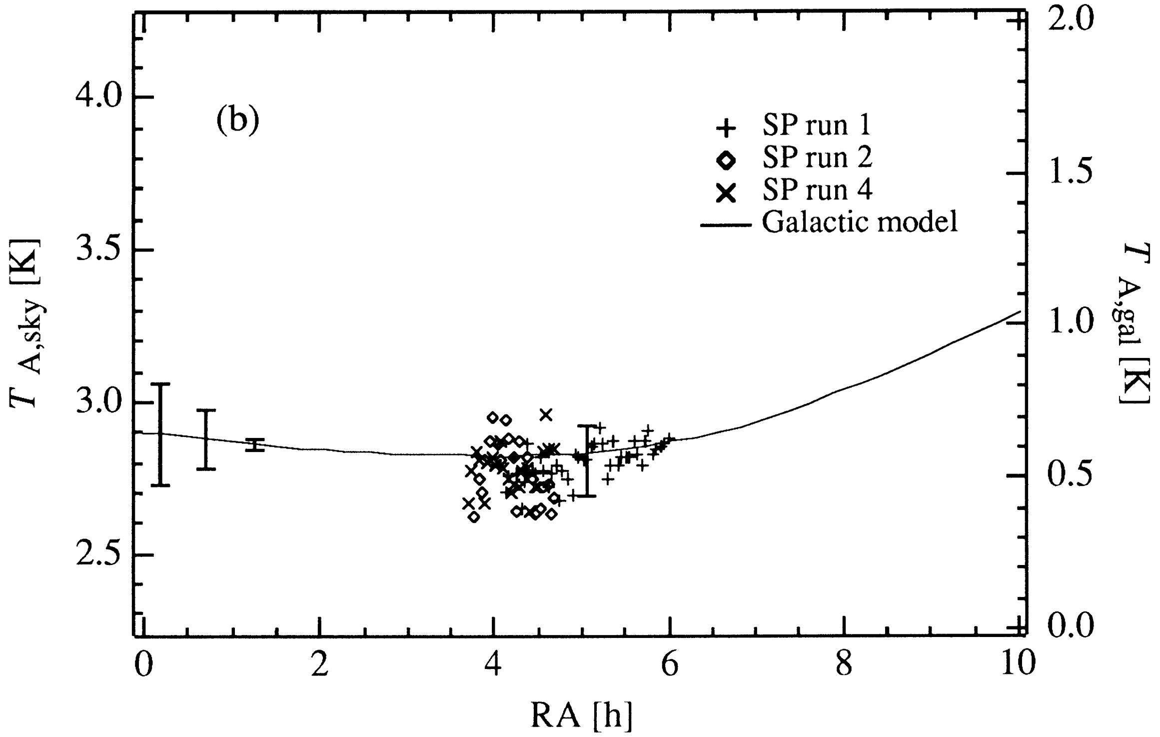
(b)
+ SP run 1
◇ SP run 2
× SP run 4
Galactic model
$T_{\mathrm{A,sky}}$ [K]
$T_{\mathrm{A,gal}}$ [K]
RA [h]
4.0
3.5
3.0
2.5
2.0
1.5
1.0
0.5
0.0
0
2
4
6
8
10

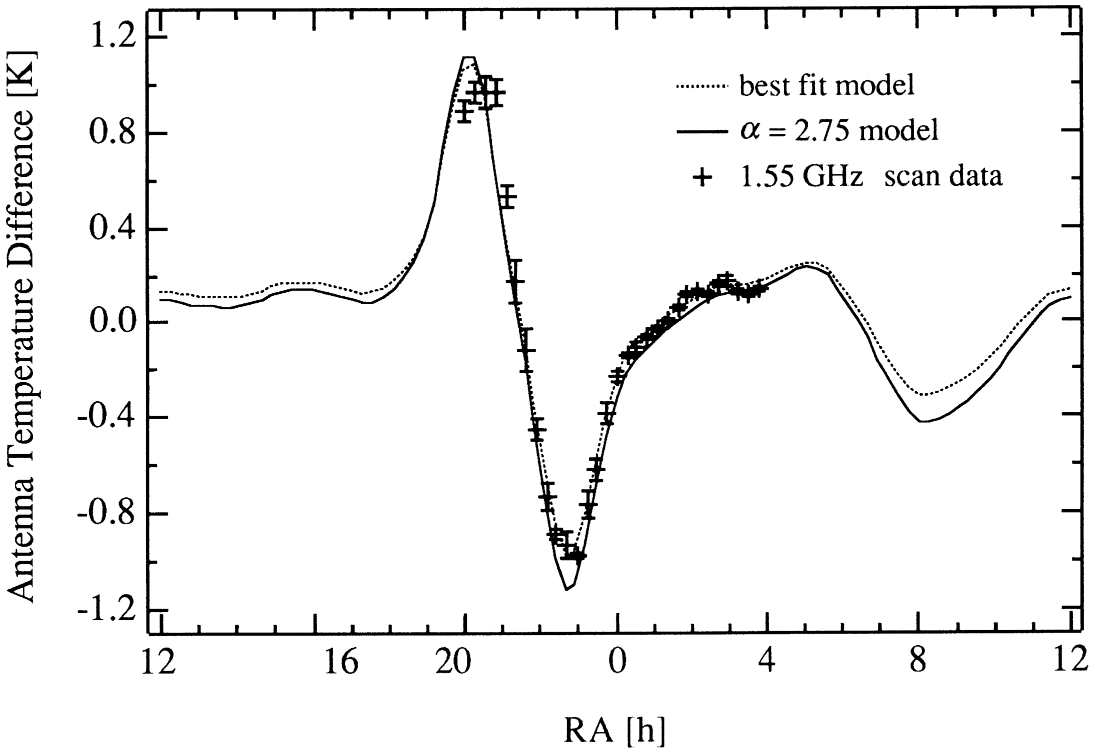
best fit model
α = 2.75 model
1.55 GHz scan data
Antenna Temperature Difference [K]
1.2
0.8
0.4
0.0
-0.4
-0.8
-1.2
12
16
20
0
4
8
12
RA [h]

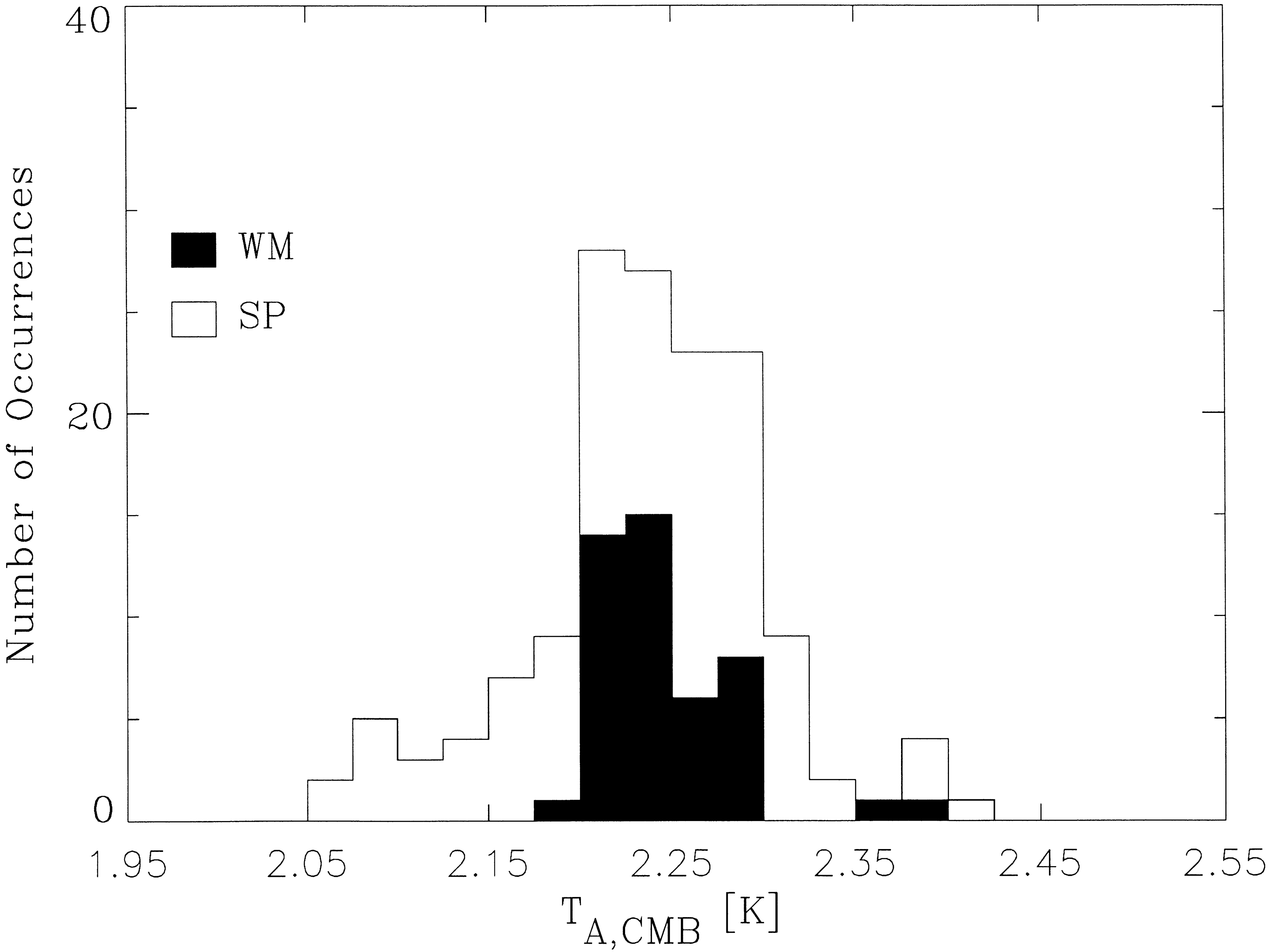
40
20
0
Number of Occurrences
WM
SP
1.95
2.05
2.15
2.25
2.35
2.45
2.55
$T_{A,CMB}$ [K]

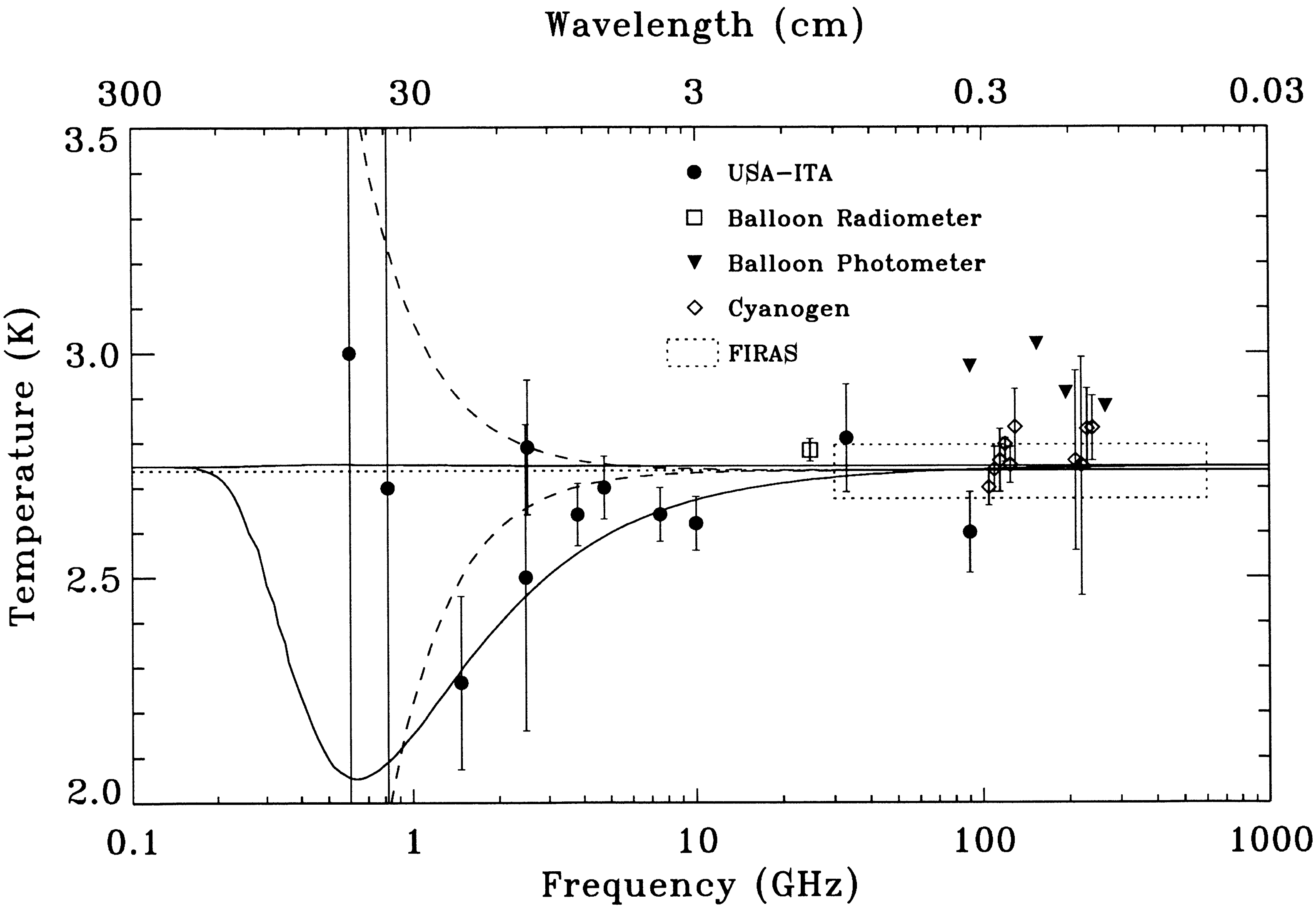
Wavelength (cm)
300
30
3
0.3
0.03
USA-ITA
Balloon Radiometer
Balloon Photometer
Cyanogen
FIRAS
Temperature (K)
3.5
3.0
2.5
2.0
0.1
1
10
100
1000
Frequency (GHz)